Understanding the Scaling of Illicit Plutonium Production in D-T Fusion Reactors

Princeton University Physics Department Spring Junior Paper

Greta Li

April 29th 2025

Abstract

An unlikely but serious concern about deuterium-tritium (DT) fusion reactors is their potential use for transmuting fertile materials into fissile materials, which could then be enriched to become weapons-grade. One scenario is the introduction of uranium-238 into the blanket, or an outer wall structure of the reactor, in order to breed plutonium-239. To assess this proliferation risk, understanding the dependency of illicit fissile mass production on secretly introduced fertile mass is crucial. In this junior paper, we explore this dependency for Pu-239 production on initial U-238 mass using a slowing-down Monte Carlo neutron simulation. In particular, we demonstrate a nonlinear dependence found in recent studies and determine that the nonlinearity stems from the saturation of Pu-239 production at the lower resonance peaks of the U-238 radiative absorption spectrum. We find that the Pu-239 production rate has an asymptotically linear behavior for large masses.

great!

Advisor: Professor Robert Goldston
Second Reader: Professor Suzanne Staggs

This paper represents my own work in accordance with University regulations.
/s/ Greta Li

1 Introduction

Fusion reactors do not consume or produce fissile materials like uranium-235 or plutonium-239 in order to operate, which makes them an attractive, non-proliferative alternative to fission reactors. Currently, deuterium-tritium (D-T) plasmas are well studied due to their favorable reaction rate versus temperature curve compared to other possible fusion reactions. Most magnetically confined fusion devices are based on the D-T reaction,

$$\mathrm{D} + \mathrm{T} \rightarrow {}^{4}\mathrm{He}\ (3.5\ \mathrm{MeV}) + \mathrm{n}\ (14.1\ \mathrm{MeV}) \tag{1}$$

However, naturally occurring tritium is rare, and fusion reactors must be able to produce tritium in order to be self-sustaining. A popular concept to breed tritium is to use molten salt blankets, or structures surrounding the reactor walls that leverage fusion neutrons to react with lithium salts to produce tritium. These blankets also remove heat from the system and reduce the irradiation of the reactor walls. [1] Lead and beryllium are often used as neutron multipliers in these blankets to boost the amount of tritium produced. [2]

Although D-T fusion reactors have limited proliferation risk due to the lack of fissile materials present (if used as intended), it is important to seriously consider the ways that they could be misused. [2] The D-T fusion reactors and neutron-multiplier materials can serve as a strong neutron source to transmute fertile material introduced secretly in the blanket into fissile material, which can then be processed for use in nuclear weapons. An example is the transmutation of uranium-238 into plutonium-239 via the following reaction chain,

$$^{238}\mathrm{U}(n,\gamma) \rightarrow {}^{239}\mathrm{U} \rightarrow_{23.5\ \mathrm{min},\beta^-} {}^{239}\mathrm{Np} \rightarrow_{2.35\ \mathrm{days},\beta^-} {}^{239}\mathrm{Pu} \tag{2}$$

where (n,γ) refers to a radiative capture reaction. [1] The International Atomic Energy Agency (IAEA) defines a significant quantity (SQ) of fissile material to be "the approximate amount of nuclear material for which the possibility of manufacturing a nuclear explosive device cannot be excluded," which also accounts for unavoidable losses due to conversion and manufacturing. [3]

In order to predict how quickly a D-T fusion reactor could produce one SQ of Pu-239, 8 kilograms, it is advantageous to understand how the Pu-239 production scales with initial U-238 mass in the blanket. Previous studies have concluded that the dependence is linear, [2], but more recent studies demonstrate a nonlinear dependence. [1, 4]

In this paper, using a slowing-down simulation, we are able to demonstrate this nonlinear dependence and pinpoint the saturation effect at the resonance energies of U-238 radiative absorption spectrum. Section 2 reviews the nonlinear behavior in Ball *et al.* using their scripts and testing for temperature dependence. [1] Section 3 covers the blanket material composition, the underlying physics of nuclear reactions, and the general workings of the slowing-down simulation. In Section 4, we present our findings: an example of the absorption spectra from a single mass run, a comparison of the tritium breeding ratio to the literature, a demonstration of the nonlinear

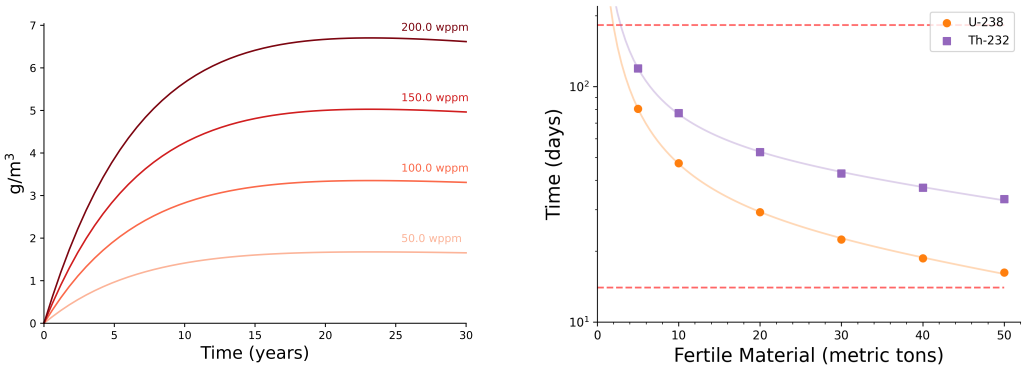

(a) Independent Depletion (b) Dependent Depletion

Figure 1: We show plots from Ball's paper that indicate a nonlinear effect. [1] The left image is the plot of Pu-239 mass density for varying levels of naturally occurring uranium impurities. The right image shows the time to one SQ for larger amounts of introduced fertile material.

behavior of Pu-239 production rates with respect to initial U-238 mass, and the saturation effect at the U-238 absorption resonances. We then briefly discuss our results and further extensions of this work in Section 5.

2 ARC-Reactor Nonlinearity

The most recent evidence for nonlinear dependence comes from Ball *et al.* who use a time-dependent depletion simulation for the blanket material on a ARC-class tokamak design. [1] We study this author's approach more closely because there is major nonlinear behavior and their scripts are publicly accessible. As a brief overview, Ball *et al.* use a depletion process that is time-dependent for a self-consistent fissile-breeding simulation. That is, they account for blanket material evolution, radioactive decays of unstable nuclei, neutron reactions on fission products, and other time-dependent effects.

A key example of nonlinearity comes up when comparing the Pu-239 production rates for two regimes of blanket composition: large amounts of fertile mass and naturally occurring amounts of fertile mass. For Fig. 1a, they use an independent depletion calculation with the naturally occurring amounts of uranium impurities. This calculation assumes that the blanket's neutron flux spectrum is constant over time due to the small amounts of fertile and fissile material.

We are mostly interested in the plutonium production before the uranium inventory is significantly depleted, so we find the initial plutonium production rate. At an impurity of 200 weight parts per million (wppm), which is equivalent to 9.6 kg of initial natural uranium mass, we find a Pu-238 mass density of 0.624 g/m^3 at 0.6 years. The total blanket volume of the ARC-design

is 342 m^3, so 1 g/m^3 is 0.342 kg. So, for an initial rate R,

$$R_{\text{ind, 9.6kg}} = 0.355 \text{ kg/yr} \tag{3}$$

where the subscript *ind* for independent and *dep* for dependent will denote the specific depletion process used to obtain these rates.

For Fig. 1b, due to the large amounts of fertile material on the order of metric tons, they use a dependent depletion calculation that accounts for the perturbation of the neutron flux spectrum due to the material's evolution in time. From the provided data, we find a time to a significant quantity (8 kg) of 22.42 days for 30 tons of initial depleted U-238 mass and 80.35 days for 5 tons of initial depleted U-238 mass. Assuming a near-constant rate of production since we are working in the time scale of days, the initial Pu-239 production rates are

$$R_{\text{dep, 5t}} = 36.34 \text{ kg/yr} \quad R_{\text{dep, 30t}} = 130.24 \text{ kg/yr} \tag{4}$$

If we were to linearly scale up the independent depletion rate from 9.6 kg to 5 tons, the rate would increase by a factor of 520. The expected rate of 184.90 kg/yr is nearly five times larger than the simulated dependent depletion rate. Likewise, for 30 tons, using a linear scaling of independent depletion rate from 9.6 kg to 30 tons, the expected rate of 1109.4 kg/yr would indicate that the independent depletion calculation for the smaller mass is nearly 8.5 times more efficient per mass.

Regarding this nonlinear effect, Ball computes the one-group cross section, which integrates over the flux spectrum and cross sections in energy to compute the breeding reaction rates. [1] The one-group cross section for the U-238 radiative capture reaction, which essentially measures the efficiency of this reaction per incident neutron per target atom, decreases as more uranium is added. Ball concludes that the nonlinearity as evidenced by the one-group cross section change is due to a substantial energy self-shielding effect as U-238 increases, but does not identify the specific physical mechanism for this effect. In a previous iteration of the paper, he attributed differences of phenomena compared to previous literature to the material evolution, such as the delay in the Np step in Eqn. 2. For the purposes of this paper, we would like to know where and why this energy self-shielding effect occurs.

2.1 Temperature

The materials in a fusion reactor are not room-temperature, but Ball uses room-temperature blanket material. We are interested in whether this nonlinearity persists in their depletion calculations even at higher temperatures.

We test three temperatures: 300K, 600K, and 900K. The first temperature is used for direct comparison with Ball's plots since room-temperature is their default. For dependent depletion scans of the time to SQ in Table 1, we find that changing the temperature cannot totally account

for this nonlinear scaling effect. As temperature increases, the time to one SQ decreases, but not substantially enough to account increase the efficiency by 5 or 8.5 times.

	5 tons of U-238	30 tons of U-238
T = 300K	81.52 days	23.31 days
T = 600K	77.32 days	21.84 days
T = 900K	75.77 days	21.13days

Table 1: We calculate the time to one significant quantity for different masses and temperatures. We note that these values are close to the provided times to one SQ for the room temperature runs of 80.35 days and 22.42 days for 5 tons and 30 tons respectively. The discrepancy in time for 300K between Ball's reported values as seen in Fig. 1b and the values in this table can be explained by our use of 10 batches of neutrons instead of 100, which will increase the statistical uncertainty.

For the independent depletion scan, we vary the temperature, but the Pu-239 mass densities with respect to time are relatively consistent with each other. We plot an example for 200 wppm in Fig. 2a. For larger uranium masses on the order of metric tons, we note that increasing the temperature increases the initial plutonium production rates as seen in Fig. 2b. However, this effect still does not boost the production rates to totally account for the nonlinear scaling.

2.2 Depletion Type

Due to the difference in depletion scripts that we used to observe a nonlinear effect, we now confirm that the nonlinear scaling is independent of depletion type. The depletion processes differ in terms of set-up and uranium type. The independent depletion process uses natural uranium (99.275% U-238, 0.720% U-235, 0.005% U-234) while the dependent depletion process uses depleted uranium (100% U-238).

We run independent depletion for wppms corresponding to natural uranium masses comparable to the dependent depletion cases. The masses they correspond to below are below,

$$m \in \{9.4, 18.9, 94.6, 189.5, 961.1, 1957.8, 11490.9, 29363.6\} \text{ (kg)} \tag{5}$$

Fig. 2b shows the initial Pu-239 production rates for different initial U-238 masses in kilograms. The smaller masses are clustered at the lower end, but we chose a linear axis scale to more clearly show the nonlinear behavior. Evidently, the difference between natural uranium and depleted uranium is not the origin of the nonlinear effect. We do note that the production rates for the larger masses are higher than the dependent depletion analysis, which leads to a lessening of the nonlinear effect. This could be due to our averaging over 0.6 years or the scaling issue for larger masses (30 tons specifically) where doubling the uranium wppm did not double the initial uranium mass. To the best of our knowledge, this was due to a defect in the independent depletion code which was not intended to handle such large masses.

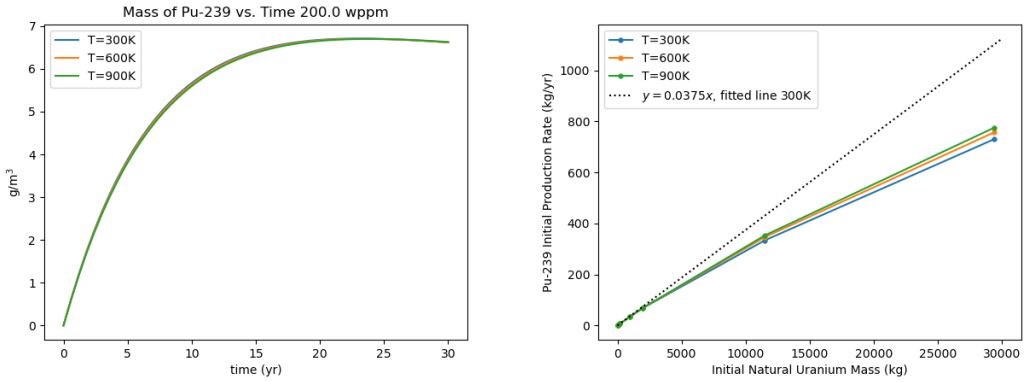

(a) (b)

Figure 2: We vary temperatures with the provided independent depletion process scripts. To the left, we simulate the evolution of the mass density of Pu-239 versus time for a natural uranium impurity of 200 wppm. To the right, we calculate the initial Pu-239 production rates for initial uranium masses up until 30 metric tons.

3 Slowing Down Simulation

To independently demonstrate the nonlinearity dependence of fissile material production from U-238 density, we use a Monte Carlo neutron slowing-down code. Our N-particle code is meant as a simple, heuristic device to probe energy regions where neutrons are absorbed. Whenever possible, we will be explicit about the approximations we make. For example, we assume that the blanket material does not evolve in time and neutrons from fission neutrons are produced at a constant energy rather than from the experimental energy distribution of fission products. Other more advanced neutron transport codes exist, such as the Monte Carlo N-Particle Transport (MCNP) code developed by Los Alamos National Laboratory [5] and OpenMC, which is an community-developed open-source code [6] used by Ball.

The Monte Carlo method leverages discretization and randomness to numerically model a given system. We generate a source of neutrons, some N particles with a given energy distribution. We also assume isotropic space where the blanket material is constant everywhere. This allows us to ignore the position of the neutrons and the physical blanket structure. Although the blanket structure does have a major impact on the neutron transport, this assumption is necessary to reduce the computational complexity of the problem. The purpose of the code is to "slow down" each neutron by calculating the relative probability of possible reactions at the neutron's energy and then randomly picking an event to simulate. Broadly speaking, the neutron outcomes at each step are either absorption or loss of energy. This process is iterated until the neutron undergoes an absorption event or reaches a negligible energy. For sufficiently high numbers of particles N, this method provides accurate statistical information on the system.

3.1 Material

We fill all space with the molten salt FLiBe, same as in Ball's ARC-reactor. FLiBe consists of lithium fluoride (LiF) and beryllium fluoride (BeF_2) in a 2:1 stoichiometric proportion.

FLiBe has properties that make the mixture advantageous for breeding blanket material in fusion configurations. First, the lithium can react with a neutron to produce tritium as shown in Eqn. 11. The produced tritium could then be extracted and released into the plasma to replenish the tritium used in the D-T fusion reaction. Second, the beryllium serves as a neutron multiplier, which increases the number of neutrons that could react with lithium to produce tritium. Neutron multiplication is necessary to replenish the loss of neutrons due to parasitic absorption and compensate for the losses of tritium due to processing after extraction from the blanket. The tritium breeding ratio (TBR) is defined as ratio of tritium atoms bred in blankets to the tritium atoms consumed in the plasma. These two properties allow for the reactor's TBR to exceed unity, which is necessary for tritium self-sufficiency in a fusion reactor and for create extra tritium for new plants. Lastly, FLiBe has already been well studied in previous fission experiments. The Molten Salt Reactor Experiment (MSRE) at Oak Ridge National Laboratory studied the practicality of this salt with fertile and fissile material dissolved in it as a fuel and coolant in nuclear reactors, finding that the salt was stable under reactor conditions and the reactors were potential economical breeders due to its fuel utilization advantages. [7]

In order to have comparable results to Ball's ARC-reactor, the relative densities in the blanket material must be the same. Ball sets a maximum molar density of 0.0181 for UF_4 in the blanket material, which corresponds to 50 metric tons of U-238 that they say is in accordance to fuel molar concentrations in fission molten salt reactor (MSR) designs. [1] Uranium-238 is typically introduced into these molten salt reactor systems as uranium tetra-fluoride. Let the molar fraction of UF_4 be ρ_U. For simplicity, we assume that the fluorine from the uranium tetra-fluoride does not impact the overall system due to its small molar percentage.

FLiBe occupies the rest of the material for a total molar fraction of $1 - \rho_U$. The element densities of FLiBe is 4F:2Li:1Be. The isotopes involved are Fluorine-19, Lithium-6, Lithium-7, and Beryllium-9. We can then calculate the relative densities of the blanket material as follows,

$$\rho_F = (4/7)(1-\rho_U) \quad \rho_{Li} = (2/7)(1-\rho_U) \quad \rho_{Be} = (1/7)(1-\rho_U) \quad \rho_U \equiv \rho_U \tag{6}$$

with the breakdown of ρ_{Li} into Li-6 and Li-7 by natural enrichment, with 7.5% Lithium-6 and 92.5% Lithium-7. Since 50 metric tons of U-238 corresponds to $\rho_U = 0.0181$,

$$\rho_U = [\text{mass (tons)}] \cdot \left(\frac{0.0181}{50}\right) \tag{7}$$

is the conversion between metric tons and molar fraction.

3.2 Cross Sections

In nuclear reactor physics, cross sections are useful quantities that characterize the probability of reaction between neutrons and some other species. The microscopic cross sections σ can be thought of as an effective cross-sectional area for collisions between a single source particle and a target nucleus. [8] This quantity has units of area, and we define a unit called the barn, which is equivalent to 10^{-28} m^2. The greater the microscopic cross section, the more likely the neutron will undergo a specific reaction with a target nucleus. To account for the density of the target material, we can multiply by the target number density N_t to get the macroscopic cross section $\Sigma \equiv N_t \sigma$. The mean free path of a neutron before undergoing a specific reaction with a target nucleus can be expressed as $1/\Sigma$. [8] We define the total microscopic cross section as

$$\overline{\Sigma} \equiv \sum_{r \in R} \Sigma. \tag{8}$$

where the sum is over all possible reactions $r \in R$ including all species.

For our purposes, we calculate the probability of a reaction $P(r)$ at each time step for given neutron with the following,

$$P(r) \equiv \Sigma_r / \overline{\Sigma} = \rho_r \sigma_r / \overline{\rho\sigma} \tag{9}$$

where instead of the number density N, we use the molar fraction ρ. Since the number density is directly proportional to the molar fraction and we are concerned only with the relative probabilities of reactions, this is a safe substitution.

The microscopic cross sections as a function of energy are determined via experiment and theory. We pull the cross section spectra primarily from the Evaluated Nuclear Data File (ENDF) version B-VII.1 with the exception of the Lithium-7 tritium production reaction from version B-VIII.1. [9–11] We limit ourselves to the reactions that are most pertinent to the energy range we consider and dominate the total microscopic cross sections for some species, which is shown in Fig. 3.

3.2.1 Elastic Scattering

Neutrons primarily slow down by scattering, or colliding with the blanket material nuclei. Although neutrons can scatter inelastically, we consider elastic scattering only as the dominant process in scattering due to the relative abundance of light nuclei.

We can calculate a bound on the minimum energy of the neutron after a collision with the following. [8] By conservation of energy, neutrons lose energy due to the recoil of the target nucleus. Let the initial energy of the neutron be E_0 and define the parameter

$$\alpha \equiv \left(\frac{A-1}{A+1} \right)^2 \tag{10}$$

where A is the mass number of the target nucleus. Then, the minimum energy of the neutron

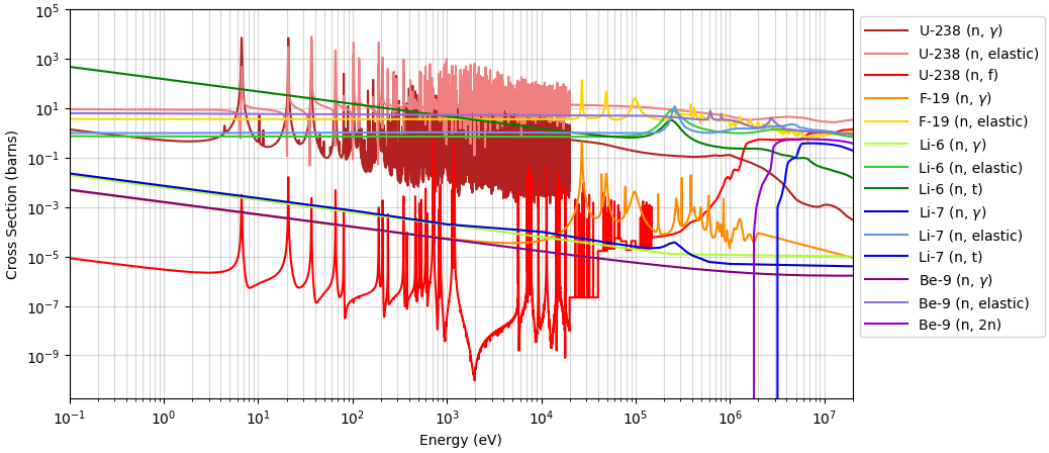

Figure 3: Microscopic cross sections of interest for the Monte Carlo slowing down simulation. Colors are roughly associated with the species, i.e. red for U-238, green for Li-6, and so on.

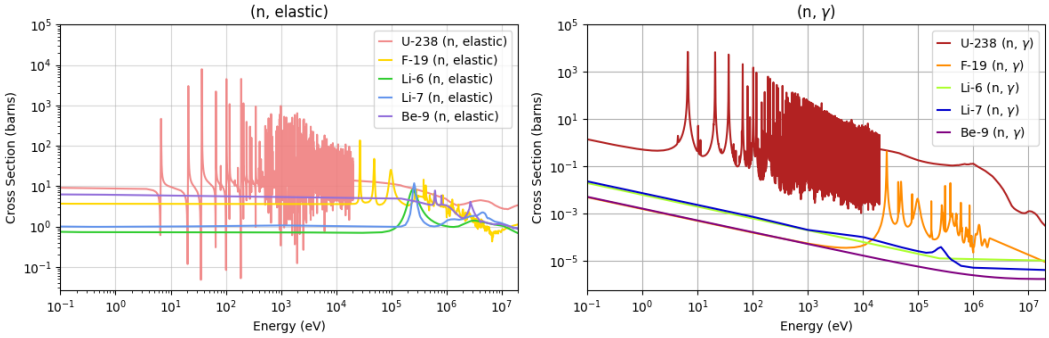

Figure 4: We isolate the elastic scattering microscopic cross sections in the left figure and the radiative capture microscopic cross sections in the right figure.

after a collision is αE_0. Naturally, the maximum possible energy of the neutron after a collision is E_0 with zero energy loss. From the fact that the probability distribution of the center-of-mass scattering angle is essentially isotropic, it can be shown that all energies in the interval $[\alpha E_0, E_0]$ are equally likely, which is equivalent to a continuous uniform distribution with respect to energy.

The relevant microscopic cross sections for elastic scattering are shown in Fig. 4. If we consider all the microscopic cross sections of interest in Fig. 3, we can see that in general, elastic scattering is more likely to occur than absorption events with the exception of U-238 radiative capture. Besides U-238 radiative capture, absorption cross sections can compete with elastic scattering for neutrons at high energies above 1 MeV and low energies below 1 eV.

3.2.2 Radiative Capture

Radiative capture, or absorption, occurs when a nucleus with atomic mass A completely absorbs a neutron to become a nucleus with atomic mass $A+1$. When de-exciting to the ground state, the nucleus emits a γ photon. [8] For this reason, this reaction is labeled as (n,γ).

We are primarily interested in the radiation absorption of U-238. This reaction has a relatively large cross section relative to the other relevant cross sections. Further, as seen in Eqn. 2, radiative capture is key to the transmutation of U-238 to the fissile material Pu-239. For simplicity, we assume that any radiative capture event on U-238 must lead to the formation of a Pu-239 nucleus. Fig. 4 shows the radiative capture cross sections for all of our species. In particular, U-238 exhibits resonance peak structures in the energy range 1 eV to 10 keV and significant $1/v$ behavior below 1 eV.

3.2.3 Fission

Although much less likely to fission with neutrons than fissile materials like U-235 and Pu-239, the fertile material U-238 can still fission with fast neutrons. Fission reactions will split the target nucleus into typically two daughter "fragment" nuclei and release particles such as neutrons, gamma rays, and alpha particles. [8] As seen in Fig. 6, the fission cross sections for U-238 are smaller than the other reactions, but are non-negligible for higher energies.

For our purposes, we are not interested in keeping track of the fission fragment nuclei. Instead, each fission event has a probability of releasing neutrons, which we will need to account for in the slowing-down process. We define $\overline{\nu}(E)$ as the mean number of neutrons released per fission event. The bar represents the sum of ν from both prompt and delayed neutrons. The spectrum for $\overline{\nu}$ is shown in the left plot of Fig. 5. The value of ν is roughly 2.5 released neutrons per fission event for most of the energy range before sharply increasing for energies greater above 1 MeV. Studies have also experimentally measured the neutron energy spectrum $\chi(E)$, which is the probability distribution of neutrons from fission of U-238. The right plot in Fig. 5 shows $\chi(E)$ for incident neutrons with energy 14 MeV. For simplicity, we will assume that all fission neutrons are released at 2 MeV, which is the approximate average energy for a born neutron.

3.2.4 Tritium Production

Both Li-6 and Li-7 are capable of reacting with neutrons to produce tritium, which is necessary for maintaining a TBR above unity. The cross sections are isolated in the right figure of Fig. 6. For lithium, the dominant absorption cross section is the Li-6 tritium-producing reaction for energies below 1 MeV. Li-7 will contribute to tritium production only in the high energy range above 3 MeV.

The Li-6 tritium-producing reaction, or (n,t) reaction, is as follows,

$$\mathrm{n} + {}^{6}\mathrm{Li} \rightarrow \mathrm{T} + {}^{4}\mathrm{He} \tag{11}$$

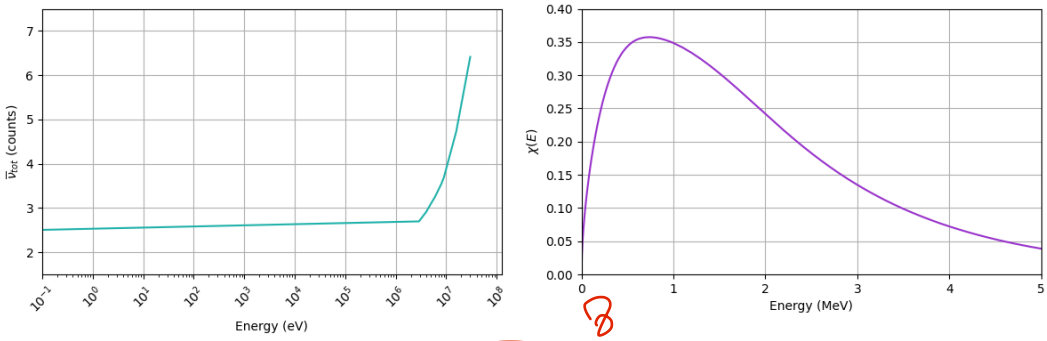

Figure 5: To the left, we plot the multiplicity distribution of neutrons $\overline{\nu}$ for U-238. To the right, we plot the energy probability distribution $\chi(E)$ for incident neutrons with energy 14 MeV on U-238 nuclei normalized to unity.

and the overall effective Li-7 (n, t) reaction is as follows,

$$\mathrm{n} + {}^{7}\mathrm{Li} \rightarrow \ \mathrm{T} + \ {}^{4}\mathrm{He} + \ n \tag{12}$$

where the alpha particle and neutron are the products from the fast decay of the primary reaction product of the lithium, He-5. [12] We will not consider the neutron byproducts of the Li-7 (n, t) reaction for our slowing-down simulation since the number of these events will be close to negligible compared to the other neutron producing reactions in our system.

3.2.5 Neutron Multiplication

Our last reaction of interest is the neutron multiplication reaction $(n, 2n)$ for Be-9. In this reaction, a Be-9 nucleus absorbs a neutron and emits two neutrons according to some neutron energy distribution. In the right side of Fig. 6, we observe that there is some cut-off energy at 1.75 MeV required for the endothermic reaction. For simplicity, we assume that the neutron products are born at the same energy and for incident neutron energy E_i, the energy E_f of the product neutrons is

$$E_f = \frac{E_i - 1.75 \text{ (MeV)}}{2} \tag{13}$$

where the remaining energy after the endothermic reaction is split between the two neutrons equally. This neutron multiplication effect is prominent for the high energy region above the cut-off energy. Below this cut-off energy, no multiplication events can occur.

3.3 Slowing Down Steps

We review our slowing-down mechanism in depth.

For our initial neutrons, we uniformly launch $200,000$ neutrons at 14 MeV. We also use an events treatment at each time step, where we choose a single reaction and species to tally. For

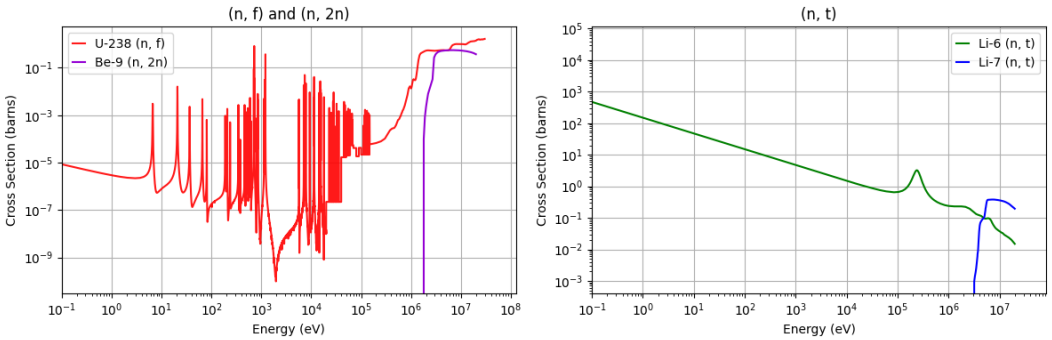

Figure 6: To the left, we have plotted the fission microscopic cross section of U-238 and the neutron multiplication of Be-9. To the right, we have plotted tritium-producing reaction microscopic cross section for both Li-6 and Li-7.

a given neutron at a given step, the neutron has some incoming energy E_i. We find the closest microscopic cross sections for all the reactions in our ENDF/IAEA data. Due to the discrete nature of the experimental data, this method introduces some error if the neutron's incoming energy E_i happens to be between a large jump in the provided energy values. To improve this, we could have used a linear interpolation between consecutive energy data points, but as seen in Fig. 3, the data looks sufficiently continuous to use this approximation.

We then calculate the macroscopic cross-sections using the relative material densities. We assume that the materials do not change in the system. That is, we will ignore the transmutation process of U-238 into Pu-239, the fission fragments of U-238, and the alpha particles in tritium-producing reactions, and any other byproducts of the radiative capture reactions. Using Eqn. 9, we can determine probability cutoffs of the events. By randomly generating a number $p \in [0, 1]$, we can probabilistically simulate an event occurring. At each step, we then return the reaction and either current energy (if absorption event) or next energy between $[\alpha E_i, E_i]$ (if scattering event for corresponding α for a chosen species).

If an absorption event occurs, we stop and record the energy bin visit. If a scattering event occurs, we proceed until the neutron is either absorbed or reaches an energy below 0.1 eV. This was a cut-off chosen as sufficiently small that there are no more events of interest. For each energy step, we can also keep track of the accumulated neutron flux spectrum ϕ, which we can approximate as the following for different energy width centered at energy E,

$$\phi(E) = n(E)v = \left(\sum_i S_0 \frac{\lambda_{\text{mfp, i}}}{v}\right) v \propto \sum_i \lambda_{\text{mfp, i}} = 1/\overline{\Sigma}(E) \tag{14}$$

where $n(E)$ is the neutron density in the zone of energy E, v is the velocity of the neutron landing at energy E, λ_{mfp} is the mean free path length, S_0 is our constant source rate term, and the total macroscopic cross section $\overline{\Sigma}$ is defined as in Eqn. 8. When we refer to summed neutron flux, we are referring to this proxy quantity without units involving time that is proportional to

the true summed neutron flux.

An issue arises in the neutron multiplication and fission neutron reactions which create further neutrons that create more neutrons and so forth. To account for these additional born neutrons on top of our initial launched neutrons, we use the following treatment.

3.3.1 Handling Neutron Multiplication Neutrons

We note that all our fission neutrons are born at 2 MeV, which is close to the 1.75 MeV Be-9 $(n, 2n)$ cut-off. The probability that any fission neutrons will then be absorbed by Be-9 is close to negligible. We are guided to handle neutron multiplication first since the born fission neutrons will not affect the Be-9 neutron multiplication of our system and the born Be-9 $(n, 2n)$ neutrons will have a nontrivial possibility of causing fission events.

The idea for handling neutron multiplication is that there are a finite number of iterations, or generations G_i of Be-9 $(n, 2n)$ neutrons. Past the cut-off energy, no more beryllium neutron multiplication events may occur. Consider the first iteration of our slowing-down simulation on the initial launched neutrons. The first generation of born neutrons due to beryllium neutron multiplication, G_1, has a maximum energy of

$$\frac{14 - 1.75 \text{ (MeV)}}{2} = 6.125 \text{ (MeV)}. \tag{15}$$

The next generation of neutrons G_2 has a maximum energy of 2.1875 MeV. The third generation of neutrons has maximum energy of 0.2 MeV, which must be our last generation. Although we are creating neutrons double the number of beryllium neutron multiplication events, this still becomes a more tractable problem. We sum all the events from our initial iteration and generations G_1, G_2, and G_3.

3.3.2 Handling Fission Neutrons

We then tally all the fission events to handle the fission neutrons. Since the born neutrons all start at 2 MeV, the challenge is in reducing the problem of infinite sum of born neutrons to a finite one.

Given N initial neutrons born at 2 MeV for a given U-238 ratio, we find an analytic expression for the fraction f of neutrons that cause fission. We numerically simulate the slowing-down scenario for different N and calculate the fraction of neutrons that cause fission. Statistically, we expect this fraction f to converge in the limit that $N \to \infty$. We see this behavior in Fig. 7a. We then fix the initial born neutrons to be $50,000$ as sufficiently large, and we vary the U-238 ratio to find f's mass dependence. In Fig. 7b, we see this relationship is close to linear, with

$$f(m) = (2.86 \cdot 10^{-4})\, m \tag{16}$$

where m is the corresponding mass for a given U-238 ratio.

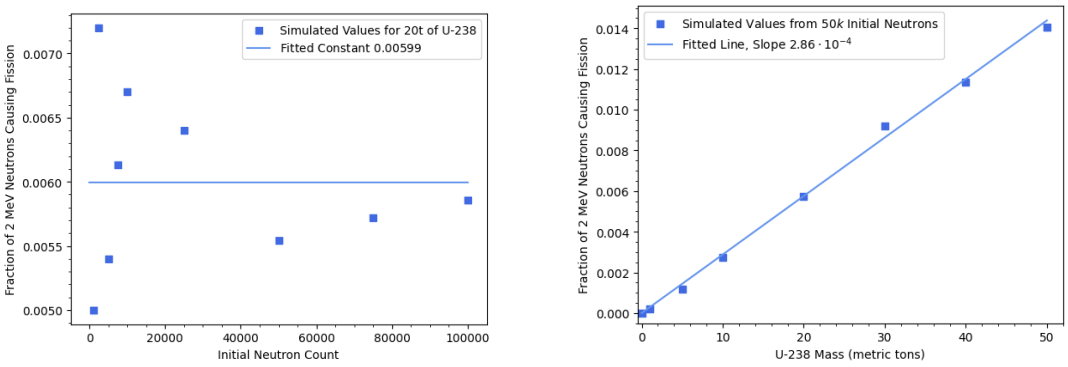

(a) Fraction f Versus Initial Neutron Count

(b) Fraction f Versus Mass

Figure 7: On the left, we fix the uranium mass at 20 tons and vary the initial neutron count. On the right, we fix the initial neutron count at $50,000$ and vary the uranium mass.

From the accumulated events of the initial iteration and three neutron multiplication generations, we can use $\overline{\nu}(E)$ to calculate the average number N_f of neutrons born at 2 MeV for the first generation of fission neutrons. A fraction of those, fN_f will fission. If we assume that all further fission events will only create one neutron at 2 MeV instead of according to the multiplicity distribution $\overline{\nu}(E)$, then f^2N_f will fission in the next generation. We will justify this approximation directly after the derivation. The infinite sum of born neutrons can be reduced using the geometric series formula,

$$N_{\text{tot}} = \sum_{k=0}^{\infty} f^k N_f = \frac{N_f}{1-f} \tag{17}$$

where the mass dependent parameter f is always less than 1, which gives a closed form solution for the total number of fission neutrons. We then simulate slowing-down on N_{tot} and add these events to the events found from the initial iteration and three neutron multiplication generations.

We now justify the assumption that all further fission events only create one neutron at 2 MeV, which has an under-estimation effect on the true N_{tot}. First, N_f is the result of using the multiplicity distribution for fission events that occur at energies above 3 MeV. The average number of birthed neutrons for energies above 3 MeV rises sharply. Then, propagating N_f as the first term, even though our neutrons will be born at 2 MeV, will have a over-estimation effect on N_{tot}. Second, the fraction f is close to negligible, since the maximum fraction corresponding to 50 tons is $\approx 1.5\%$.

4 Simulation Results

Here, we present and analyze results from our slowing down simulations. In particular, our simulation demonstrates nonlinearity of Pu-239 production with respect to U-238 initial mass as

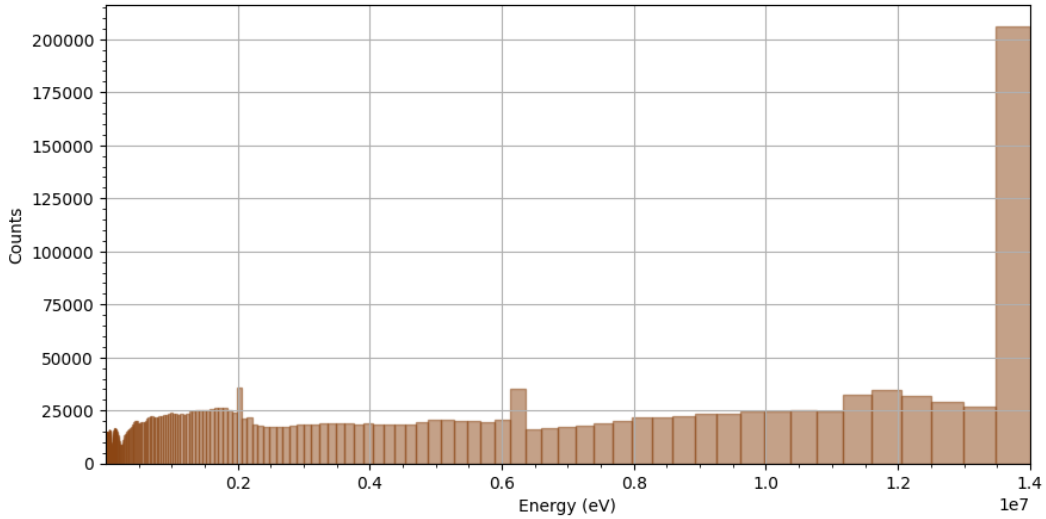

Figure 8: We plot the summed neutron flux $\phi(E)$ in 500 logarithmically spaced bins between 0.1 eV and 14 MeV for a single slowing-down run for 20 tons of U-238.

seen in Ball et al. We first give an example of the slowing down simulation for a single mass. In order to examine the nonlinearity, we run the slowing down simulation for multiple masses m

$$m \in \{0.1, 1, 2.5, 5, 10, 20, 30, 40, 50\} \text{ (metric tons)} \tag{18}$$

where the larger masses are chosen specifically to match Ball's choice of masses. We check the rate of growth of Pu-239 production across our entire slowing-down energy range to find any saturating regions where nonlinear growth of Pu-239 occurs. We find that the saturation occurs for the lower energy region below 1 keV, which corresponds to the large U-238 absorption resonances. Note, we have assumed that every U-238 radiative absorption event directly results in a Pu-239 production event. We also calculate the tritium breeding ratio and explore the implications of this nonlinearity behavior.

4.1 Single Mass Run

We plot relevant quantities for the case of 20 metric tons of U-238: summed neutron flux over all species and absorptions spectra for individual species.

For the summed neutron flux in Fig. 15, we sort our total energy bin visits into a histogram, weighting each visit by the neutron flux given by Eqn. 14. We include the initial energies of the neutrons, which explains the large peak at 14 MeV. We see smaller peaks at 6.1 MeV and 2 MeV, which correspond to the neutrons born from the neutron multiplication events. Although those values are the approximated maximum energies of generations, the majority of the neutron multiplication atoms will be born around these values. Neutrons are more likely to

be absorbed where there is a large influx of neutrons, and our initial iteration launched neutrons from the same energy. We also observe a modest increase in neutron flux around 12 MeV. Based on the absorption visits, this appears to be an effect from the sharp drop-off in Be-9 neutron multiplication and Li-7 tritium production cross sections.

We make a few observations on the absorptions spectra for the individual species, which is shown in Fig. 9. For the radiative capture reactions, we can see the structure of the resonances (i.e. the sharp peaks), especially for U-238 and F-19. Although the respective microscopic cross sections increase as energy decreases, the neutron counts taper off in our simulation. This is due to the finite number of neutrons which are absorbed before reaching these lower energies. We have also omitted the spectra of Li-6 radiative capture since there were no events. The Be-9 radiative capture spectra is also close to negligible. For the tritium reaction (n, t), Li-7 contributes for the upper energy range above 4 MeV, but Li-6 contributes to the bulk of the system's Lithium production with the abundance of events at lower energies. We also note that fission events primarily occur above 1 MeV, which is explained by the peak of the U-238 fission microscopic cross section there.

4.2 Tritium Breeding Ratio

We can calculate the tritium breeding ratio (TBR) for our system to confirm that it is within reason. We assume that neutrons that are initially launched are products of D-T reactions in the fusion reactor. So, for every neutron initially launched, one tritium atom is consumed in the plasma. To find the TBR of our system, we find the number of tritium-producing events, which are due to Li-6 and Li-7 (n, t) reactions, and divide by the number of initial launched neutrons, $200,000$.

We plot the TBR values for varying U-238 mass in Fig. 10b. As Ball remarks, we expect the TBR to monotonically decrease with respect to uranium mass. [1]. Physically, increasing uranium means that more neutrons will proportionally fission or be radiatively captured by uranium while the amount of lithium decreases. We do see a monotonic decreasing relation for smaller uranium masses, but then the TBR levels off for masses greater than 20 tons. This could be due to statistical noise as the values oscillate. From Fig. 10a, we also note that our simulated TBR values range from 1.365 to 1.395 while the ARC-reactor TBR values cover a slightly wider range from 1.12 to 1.175. As of 2020, the best estimate for an achievable TBR for a detailed blanket system was 1.15, [13] so our TBR values are not physically realistic. However, in assuming isotropic space, we did not simulate a blanket configuration, which would have included neutron loss in leaks or absorption in the tungsten and V-4Cr-4Ti wall layers. We also used a one-pass process, whereas neutrons in an ARC-class reactor could collide out of the blanket and potentially re-enter the blanket. Accounting for these factors would lead to a decrease in our simulated TBR.

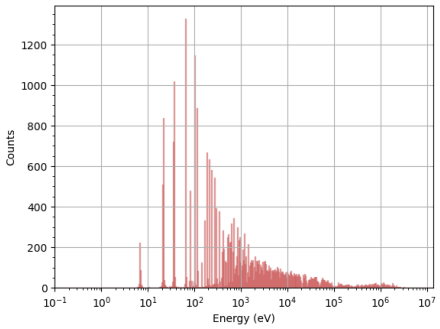

(a) U-238 (n, γ)

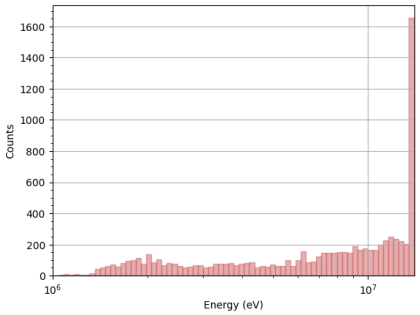

(b) U-238 (n, fis)

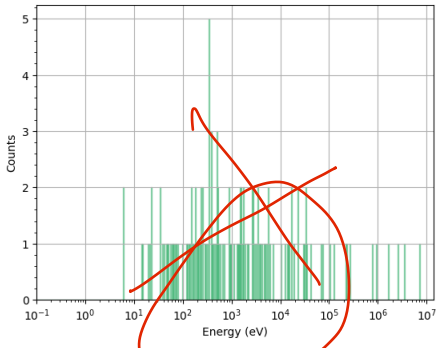

(c) Li-6 (n, γ)

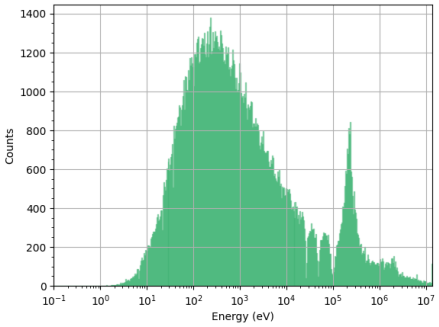

(d) Li-6 (n, t)

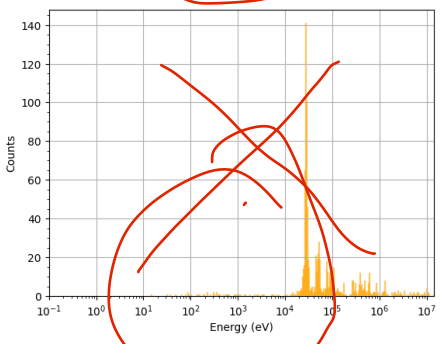

(e) F-19 (n, γ)

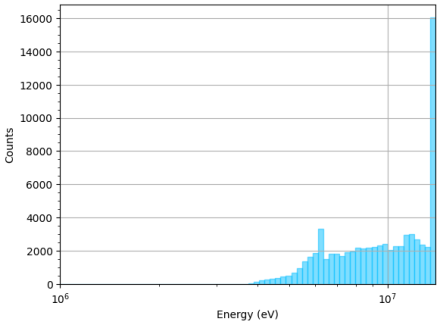

(f) Li-7 (n, t)

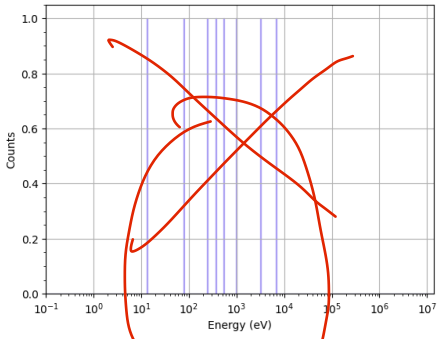

(g) Be-9 (n, γ)

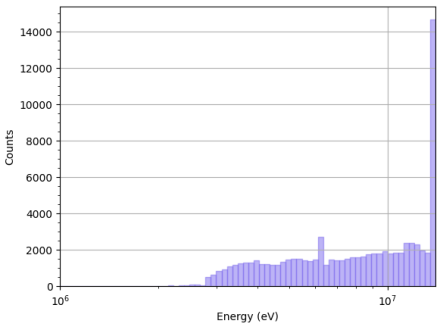

(h) Be-9 $(n, 2n)$

Figure 9: Absorption Spectra for 20 metric tons of U-238.

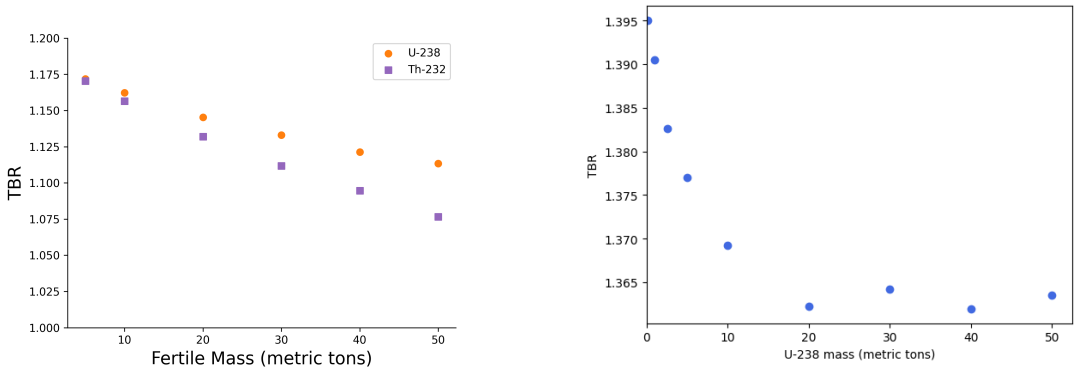

(a) (b)

Figure 10: To the left, we have Ball's plot of TBR versus fertile mass of both U-238 and Th-232. To the right, we have our slow-down simulation's TBR versus fertile mass of U-238.

4.3 Slow Down Nonlinearity

We revisit the question of nonlinearity. Intuitively, if there was a linear dependence of Pu-239 production on U-238 mass, then doubling the amount of initial fertile mass would double the Pu-239 production, whether that be U-238 radiative capture event counts or Pu-239 production rate.

We find a nonlinear dependence in our slowing-down simulation. Pu-239 production is proportional to the number of U-238 radiative capture events per launched neutron. This quantity was calculated over varying U-238 masses in Fig. 11b. We can fit a line to the Pu-239 production for larger masses greater than 20 metric tons, but the smaller masses do not fit well to this line. The same qualitative nonlinear behavior is found using Ball's independent depletion simulation, which we plot again in Fig. 11a. We include the line fitted to the first three masses (10.4 kg, 18.9 kg, 94.6 kg) to show the nonlinear behavior. Note, in the independent depletion, we approximate to find the Pu-239 initial production rate in kg/yr while the slowing-down simulation has no time units. If we extend our neutron source into a rate by relaunching our neutrons every second and still enforcing that the material evolution is time-independent, we see that the independent depletion results and our slowing down simulation results are comparable.

Further, we can divide the number of U-238 radiative capture events per launched neutron by the mass, as seen in Fig. 12a. If we compare this quantity for 0.1 tons and 30 tons, we see that the 0.1 tons of U-238 is nearly $0.0162/0.00588 \approx 2.756$ times more efficient per unit mass. From the independent depletion simulations, 0.1 tons had an initial rate of 3.55 kg/yr while 30 tons had an initial rate of 730.2 kg/yr. In scaling 0.1 tons to 30 tons, the expected rate is $3.55 \cdot 300 = 1065$ kg/yr, which is 1.46 times more efficient than the simulated value. Granted, our slow-down simulation assumes isotropic space and constant blanket material densities, but this calculation indicates that our nonlinear behavior is roughly comparable to the behavior in Ball's independent depletion process.

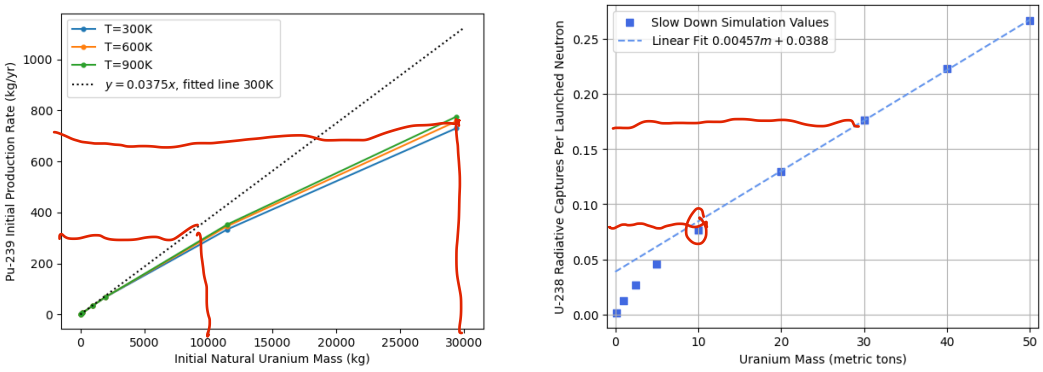

(a) (b)

Figure 11: We observe nonlinear behavior in the plutonium production-related quantities versus initial mass for both independent depletion simulation and our slowing-down simulation. On the left for the independent depletion simulation, we plot the initial Pu-239 production rate up until 30 metric tons. On the right for the slowing-down simulation, we plot the number of U-238 (n, γ) events per launched neutron up until 50 metric tons.

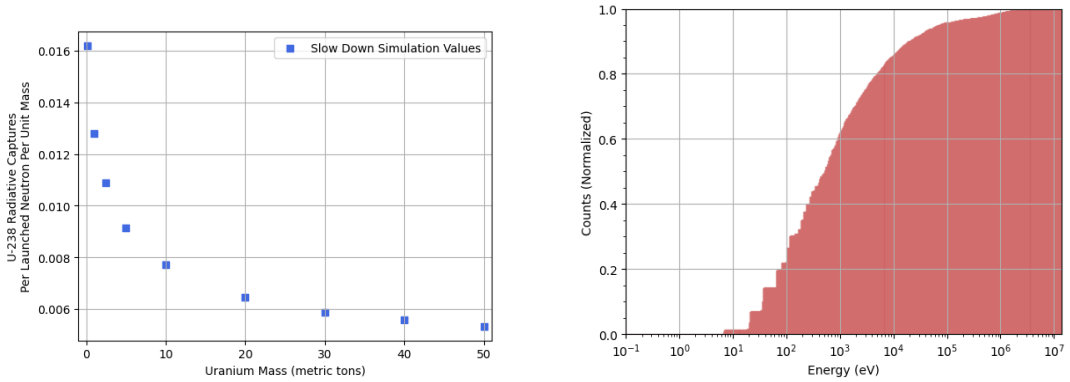

(a) (b)

Figure 12: To the left, we have plotted the mass dependence of U-238 radiative capture counts per launched neutron per unit mass. To the right, we have plotted the integrated and normalized U-238 radiative capture spectrum for 20 tons of initial uranium.

4.4 Saturation of Energy Bins

Since the overall plutonium production with respect to U-238 mass exhibits sub-linear growth, we are interested in finding the specific energy regions where the plutonium production "saturates," or does not increase linearly with uranium mass.

The intuition comes from looking at the integrated U-238 (n, γ) spectrum normalized to unity, such as for 20 tons in Fig. 12b. If there was a linear dependence, we would expect this spectra to be the exact same across all different masses. If we remove the normalization, we would expect the shape to remain the same, but the vertical axis to scale linearly with the mass. Since there is nonlinear behavior where the efficiency of plutonium production decreases as mass increases, some energy range, or bin, must also have sub-linear growth.

For each given U-238 mass, we bin our U-238 radiative capture events, or Pu-239 production event spectra by dividing the energy range logarithmically by half powers of ten. We then plot the Pu-239 production with respect to U-238 mass for each of these bins as shown in Fig. 13. Since the counting experiment distributions are nearly Poisson, the uncertainty of each bin is close to the square root of the counts. The bin from 1 eV to 3 eV has so little counts that it has no statistical meaning, so we discard this. The bins from 3 eV to 1 keV display clear nonlinear behavior. The dependence of plutonium production on mass per bin steadily flattens to become more linear as energy increases. The bins for energy greater than 1 keV appear nearly linear. We notice that there is more noise for the highest energy bins, 3 MeV to 14 MeV, which is likely due to greater uncertainty due to low counts.

We can also plot the summed neutron flux for each mass per energy bin, as in Fig. 14. For the bins 3 eV to 300 keV, the summed neutron flux spectrum decreases as mass increases, which indicates that less neutrons are reaching lower energies per unit time. For energies from 300 keV to 3 MeV, the summed neutron flux increases close to linearly. However, the summed neutron flux decreases again for larger masses in energy bins above 3 MeV, which is indicative of greater amounts of fission events. The monotonically increasing behavior for the previous bins is likely due to the fission neutrons born at 2 MeV and the second and third generations of neutron multiplication neutrons born below 2.2 MeV.

If we look at the microscopic cross sections for the U-238 radiative capture reaction in the energy bins with saturating behavior, we notice that this is the region of the largest resonance peaks. If we then look at the neutron flux spectrum, the neutron flux decreases as mass increases, which could explain part of the saturation effects. Even with increased densities of U-238, less neutrons in an energy bins means less possible absorption events. However, we can examine the case of energy bins where the summed neutron flux is nearly constant and the Pu-239 production shows signs of saturation as the mass increases.

Consider the energy bin from 100 eV to 300 eV. The summed neutron flux decreases by a modest amount,

$$(156794.40 - 152931.15)/156794.40 \cdot 100 = 2.46\% \tag{19}$$

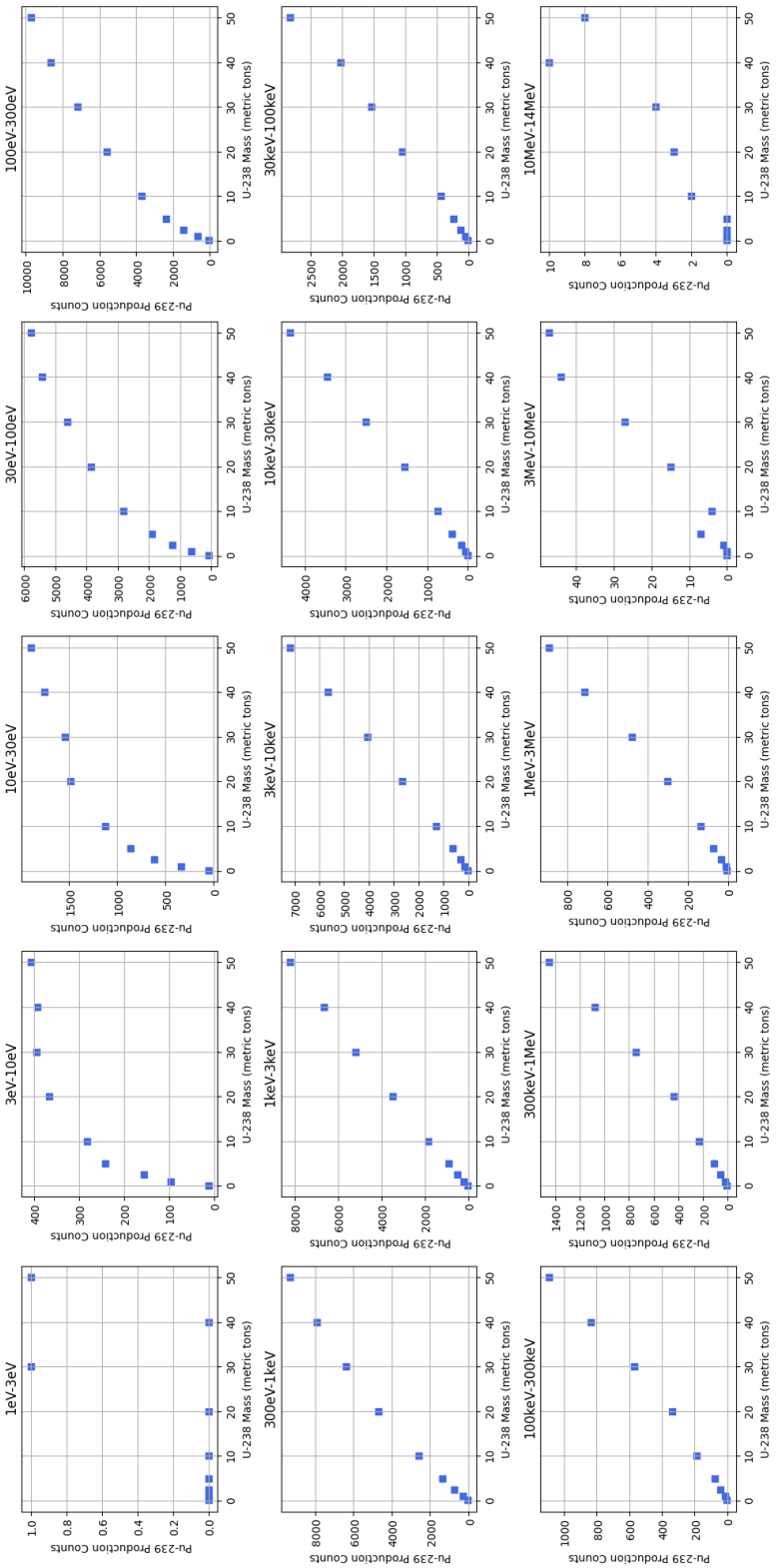

Figure 13: Dependence of Plutonium-239 Production on Mass for individual energy bins

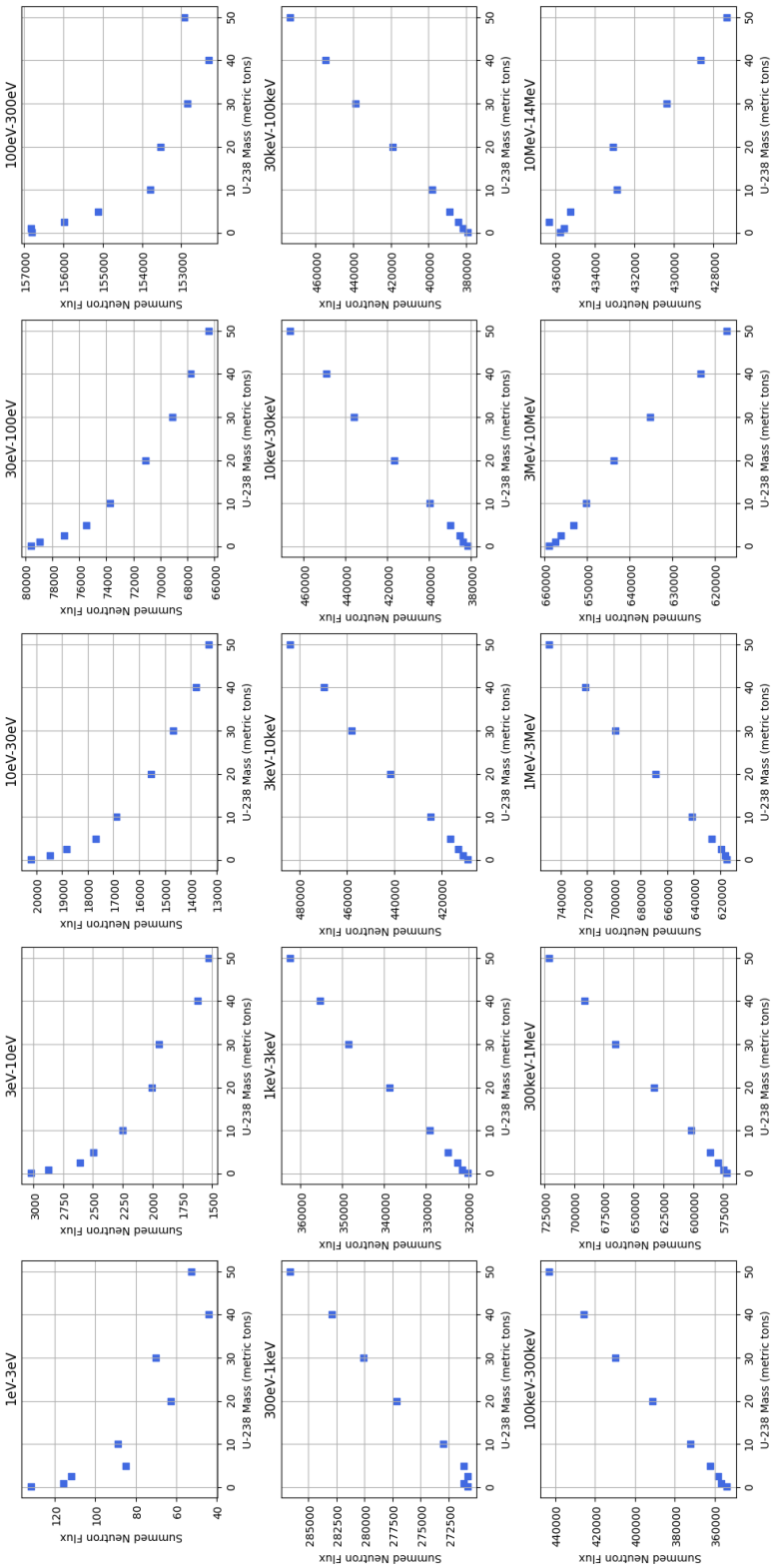

Figure 14: Dependence of Summed Neutron Flux on Mass for individual energy bins.

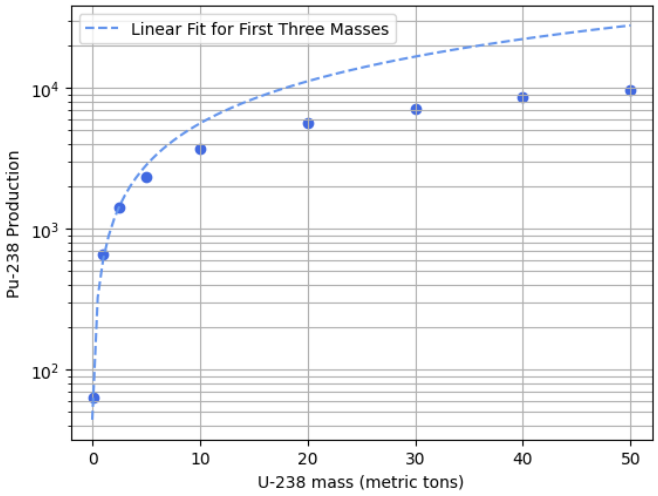

Figure 15: We plot the Pu-239 production counts for 100 eV to 300 eV along with a linear fit to the first three points. The vertical axis is in a logarithmic scale.

from 0.1 tons to 50 tons of initial U-238 mass. However, if we look at the Pu-239 production counts for the same energy bin, the simulated count at 50 tons is nearly a third less than the predicted count from a linear fit. So, the decrease in summed neutron flux cannot be the primary cause for the saturation of the Pu-239 production.

At these lower energy bins, the resonances appear to be the dominating effect for the saturation behavior. To understand this physically, we can look at an energies in a specific resonance. As mass increases, the macroscopic cross section of the U-238 radiative capture reaction increases, which boosts the probability of absorption at this energy. There are diminishing returns for increasing mass because the relative probability of U-238 radiative absorption occurring can only approach 1. Meanwhile, near an absorption peak, the blanket material is "shielded" from the neutron flux since the summed neutron flux near a resonance decreases as the mean free paths is shorter near resonance energies. [8]

We predict that the total Pu-239 production rate will have a linear asymptotic behavior, as seen in Fig. 11b. As the mass increases further, the lower energy regions will saturate to a constant. Only the linear effects of Pu-239 production above 1 keV will remain.

5 Discussion and Conclusion

In this paper, we have demonstrated the nonlinear dependence of the Pu-239 production on initial U-238 mass using a slowing-down Monte-Carlo simulation. Ball claimed that the nonlinear behavior was due to energy self-shielding. We find that saturation occurs at the lower energy resonances of U-238, which is an explicit identification of the physical mechanism of Ball's claim. Furthermore, we predict asymptotic linear behavior of the Pu-239 production as the uranium

mass grows. The advantage of the slowing-down code lies in its numerical simplicity relative to other Monte-Carlo neutron transport codes. The implications are that the nonlinearity should be present in blanket systems that gain a significant fraction of their Pu-239 production from resonances. The Pb-Li blanket system in Glaser and Goldston [2] did not demonstrate this nonlinearity, perhaps due to reduced elastic scattering of neutrons that would slow them down into the resonance region.

There are many possible further improvements and extensions to the slowing-down simulation. We could identify which U-238 resonances have the greatest saturating effect. Regarding material, we could choose a lead-lithium blanket instead, which would reduce the elastic scattering in the system, or use the fertile material Thorium-232 instead of Pu-239. We studied the temperature dependency only with Ball's OpenMC scripts, but we could test the Doppler broadening of resonances with our code. Implementing some spatial dependence or introducing some effect of a tungsten surface could lower the tritium breeding ratio to be consistent with current reactor designs. Regarding the efficiency of the code, we could reduce statistical noise further by tracking a proportionality of a chosen reaction in energy bins instead of saving entire events. These additions would not only increase the physical accuracy of our current model, but also improve the functionality of our simulation in order to test more of the general scaling dependencies of fissile production on initial fertile masses.

Slowing-Down Code

The cross-sectional text files, simulation data stored in pickle files, and Python notebooks can be found here. Images from this junior paper are found within the two notebooks `processing.ipynb` and `slowingdown.ipynb`. The paths in these notebooks to load in the pickle files may need to be adjusted.

Acknowledgments

I would like to give many, many thanks to Prof. Goldston for his patience, humor, and time over this semester. I sincerely thank Prof. Staggs for being as my second reader.

References

[1] John L. Ball, Ethan E. Peterson, R. Scott Kemp, and Sara E. Ferry. Assessing the risk of proliferation via fissile breeding in arc-class fusion power plants. *Nuclear Fusion*, 65(3):036038, feb 2025.

[2] A. Glaser and R.J. Goldston. Proliferation risks of magnetic fusion energy: clandestine production, covert production and breakout. *Nuclear Fusion*, 52(4):043004, mar 2012.

[3] International Atomic Energy Association (IAEA). *Safeguards Glossary*. Number 3 in International Nuclear Verification Series. INTERNATIONAL ATOMIC ENERGY AGENCY, Vienna, 2003.

[4] Peng Lu, Pavel Pereslavtsev, Francisco Hernandez, and Ulrich Fischer. Activation analysis for the hcpb blanket module in the european demo. *Fusion Engineering and Design*, 125:18–23, 2017.

[5] Joel A. Kulesza, Terry R. Adams, Jerawan C. Armstrong, Simon R. Bolding, Forrest B. Brown, Jeffrey S. Bull, Timothy P. Burke, Alexander R. Clark, Robert Arthur Forster, III, Jesse F. Giron, Avery S. Grieve, Colin J. Josey, Roger L. Martz, Gregg W. McKinney, Eric J. Pearson, Michael E. Rising, Clell J. Solomon, Jr., Sriram Swaminarayan, Travis J. Trahan, Colin A. Weaver, Stephen C. Wilson, and Anthony J. Zukaitis. MCNP® Code Version 6.3.1 Theory & User Manual. Technical Report LA-UR-24-24602, Rev. 1, Los Alamos National Laboratory, Los Alamos, NM, USA, May 2024.

[6] Paul K. Romano, Nicholas E. Horelik, Bryan R. Herman, Adam G. Nelson, Benoit Forget, and Kord Smith. Openmc: A state-of-the-art monte carlo code for research and development. *Annals of Nuclear Energy*, 82:90–97, 2015. Joint International Conference on Supercomputing in Nuclear Applications and Monte Carlo 2013, SNA + MC 2013. Pluri- and Trans-disciplinarity, Towards New Modeling and Numerical Simulation Paradigms.

[7] M. W. Rosenthal, P. R. Kasten, and R. B. Briggs and. Molten-salt reactors—history, status, and potential. *Nuclear Applications and Technology*, 8(2):107–117, 1970.

[8] Robert J. Goldston. The science of nuclear energy: Fission and fusion. unpublished, 2025.

[9] M.B. Chadwick, M. Herman, P. Obložinský, M.E. Dunn, Y. Danon, A.C. Kahler, D.L. Smith, B. Pritychenko, G. Arbanas, R. Arcilla, R. Brewer, D.A. Brown, R. Capote, A.D. Carlson, Y.S. Cho, H. Derrien, K. Guber, G.M. Hale, S. Hoblit, S. Holloway, T.D. Johnson, T. Kawano, B.C. Kiedrowski, H. Kim, S. Kunieda, N.M. Larson, L. Leal, J.P. Lestone, R.C. Little, E.A. McCutchan, R.E. MacFarlane, M. MacInnes, C.M. Mattoon, R.D. McKnight, S.F. Mughabghab, G.P.A. Nobre, G. Palmiotti, A. Palumbo, M.T. Pigni, V.G. Pronyaev, R.O. Sayer, A.A. Sonzogni, N.C. Summers, P. Talou, I.J. Thompson, A. Trkov, R.L. Vogt, S.C. van der Marck, A. Wallner, M.C. White, D. Wiarda, and P.G. Young. ENDF/B-VII.1 nuclear data for science and technology: Cross sections, covariances, fission product yields and decay data. *Nuclear Data Sheets*, 112(12):2887 – 2996, 2011. Special Issue on ENDF/B-VII.1 Library.

[10] National Nuclear Data Center from Brookhaven National Laboratory. Sigma cross section data, 2011. https://www.nndc.bnl.gov/sigma/index.jsp?as=238&lib=endfb7.1&nsub=10.

[11] International Energy Energy Agency (IAEA) Nuclear Data Services (NDS. Evaluated nuclear data file (endf) database versin of 2025-01-29. https://www-nds.iaea.org/exfor/endf.html.

[12] F. Brown, R.H. James, J.L. Perkin, and J. Barry. The cross section of the 7li(n, t) reaction for neutron energies between 3·5 and 15 mev. *Journal of Nuclear Energy. Parts A/B. Reactor Science and Technology*, 17(3):137–141, 1963.

[13] Mohamed Abdou, Marco Riva, Alice Ying, Christian Day, Alberto Loarte, L. R. Baylor, Paul Humrickhouse, Thomas F. Fuerst, and Seungyon Cho. Physics and technology considerations for the deuterium–tritium fuel cycle and conditions for tritium fuel self sufficiency. *Nuclear Fusion*, 61(1), 11 2020.